Structures of Gramicidins A, B, and C Incorporated into Sodium Dodecyl Sulfate Micelles[†,‡]

Lara E. Townsley,[§] W. Andrew Tucker,[||] Simon Sham,[⊥] and James F. Hinton*

Department of Chemistry and Biochemistry, University of Arkansas, Fayetteville, Arkansas 72701

Received May 8, 2001; Revised Manuscript Received July 31, 2001

ABSTRACT: Gramicidins A, B, and C are the three most abundant, naturally occurring analogues of this family of channel-forming antibiotic. GB and GC differ from the parent pentadecapeptide, GA, by single residue mutations, W11F and W11Y, respectively. Although these mutations occur in the cation binding region of the channel, they do not affect monovalent cation specificity, but are known to alter cation-binding affinities, thermodynamic parameters of cation binding, conductance and the activation energy for ion transport. The structures of all three analogues incorporated into deuterated sodium dodecyl sulfate micelles have been obtained using solution state 2D-NMR spectroscopy and molecular modeling. For the first time, a rigorous comparison of the 3D structures of these analogues reveals that the amino acid substitutions do not have a significant effect on backbone conformation, thus eliminating channel differences as the cause of variations in transport properties. Variable positions of methyl groups in valine and leucine residues have been linked to molecular motions and are not likely to affect ion flow through the channel. Thus, it is concluded that changes in the magnitude and orientation of the dipole moment at residue 11 are responsible for altering monovalent cation transport.

The gramicidin family of linear polypeptides represents a biologically viable channel system in which specific changes in amino acid composition can be correlated with cation binding selectivity and transport. A mixture of nine pentadecapeptides is produced naturally by the aerobic, sporulating bacterium *Bacillus brevis*, and the relative abundance of the different gramicidins can be controlled by the concentrations of various amino acids in the growth medium (*1*−*7*). The three major gramicidin species, A, B, and C, typically occur in a ratio of approximately 7:1:2, respectively, and have the amino acid sequence formyl-L-Val_1-D-Gly_2-L-Ala_3-D-Leu_4-L-Ala_5-D-Val_6-L-Val_7-D-Val_8-L-Trp_9-D-Leu_{10}-L-Xxx_{11}-D-Leu_{12}-L-Trp_{13}-D-Leu_{14}-L-Trp_{15}-ethanolamine, where Xxx is Trp in gramicidin A (GA),[1] Phe in gramicidin B (GB), and Tyr in gramicidin C (GC) (*6*). Three of the minor species differ from GA, GB, and GC by replacement of Val with Ile at position 1, while three are acylated forms of the major gramicidins (*2*−*5*). Further variations in amino acid sequence can be obtained by total or semi-synthesis (*8*−*10*). Because these analogues provide subtle but well-defined perturbations of the properties of gramicidin, they represent a powerful means of deciphering the structure−function relationship of this channel system. GA, the parent molecule, is arguably the best characterized model ion channel and has, to date, been the principal proving-ground for many of the ideas about the molecular nature of ion transport in membranes (*11*).

Gramicidin has been shown to induce monovalent cation permeability in both natural and artificial lipid membranes. Hladky and Haydon found that the addition of small amounts of GA to bilayer membranes caused discrete conductance changes because of the formation of channels (*12*). The channel is composed of two single-stranded, right-$\beta^{6.3}$-helices joined by hydrogen bonds between their N-termini (*13*, *14*). While the gramicidin channel exhibits appreciable selectivity between monovalent cations, this channel is essentially impermeable to multivalent cations and anions (*15*). The monovalent cation selectivity of the GA channel has been observed in single channel conductance studies, and the order of increasing conductance was found to be: $Li^+ < Na^+ < K^+$ (*16*, *17*). The kinetic activation enthalpies for the transport of these cations through the GA channel (*18*) and the cation binding affinities of the channel (*19*, *20*) are in agreement with the conductance data.

The first step in the transport process involves the binding of the cation to the channel. The binding site has been identified at the channel opening in the region formed by residues Trp_9 through Trp_{15} (pertinent references found in

[†] Funding for this project was provided by NSF Grant MCB-9313835 and NIH Grant 5P20RR15569-01.

[‡] Coordinates for Gramicidins A, B, and C have been deposited in the RCSB Protein Data Bank with accession codes 1JNO, 1JO3, and 1JO4, respectively.

* To whom correspondence should be addressed. E-mail: jhinton@uark.edu. Phone: (501) 575-5143. Fax: (501) 575-4049.

[§] Present address: Department of Chemistry and Biochemistry, University of California, Santa Barbara, CA 93106.

[||] Present Address: Department of Chemistry, Queens College, Charlotte, NC 28277.

[⊥] Present Address: Department of Chemistry, University of California, Davis, CA 95617.

[1] Abbreviations: GA, gramicidin A; GB, gramicidin B; GC, gramicidin C; d_2-TFE, deuterated trifluoroethanol (CF_3CD_2OH); d_{25}-SDS, deuterated sodium dodecyl sulfate; NMR, nuclear magnetic resonance; DQF-COSY, double quantum filtered correlation spectroscopy; TOCSY, total correlation spectroscopy; NOE, nuclear Overhauser effect; NOESY, NOE spectroscopy; DG/SA, distance geometry/simulated annealing; RMSD, root-mean-square deviation; Eta, ethanolamine; DMPC, dimyristoylphosphatidylcholine.

10.1021/bi010942w CCC: $20.00
Published on Web 09/06/2001

refs *11* and *21*). Therefore, it is not surprising to find that changes in ion−dipole interactions within the binding region are very important in modulating the transport of ions through the channel (*22*). With the replacement of the Trp_{11} (dipole moment 2.08 D) by Phe (dipole moment 0.0 D), the single channel conductance of Na^+ [1.0 M NaCl at 25 ± 1 °C and 200 mV in diphytanoylphospatidylcholine/*n*-decane bilayers (*5*, *8*)] decreases from 14.4 pS to 8.7 pS; however, substitution with Tyr (dipole moment 1.54 D) effects only a slight conductance decrease to 13.3 pS. The activation enthalpies for the transport of Li^+ through GA, GB, and GC channels incorporated into vesicles are 7.2, 8.0, and 7.3 kcal/mol, respectively (*11*). For Tl^+ binding to GA and GC channels, the corresponding enthalpies are −7.2 and −3.9 kcal/mol (*11*). Obviously, there is a complex relationship between the magnitude and orientation of the side-chain dipole moments and the monovalent cations that determines their binding and movement through the gramicidin channels.

Not only will replacement of Trp_{11} by Phe or Tyr alter the magnitude and orientation of that residue's dipole moment, but an amino acid substitution could induce variations in side-chain orientations and/or the backbone structure of the channel, which in turn could affect conductance properties. We present here for the first time a comparison of the three-dimensional structures of GA, GB, and GC incorporated into deuterated sodium dodecyl sulfate micelles in an attempt to address the question of structure modification by amino acid substitution.

EXPERIMENTAL PROCEDURES

Materials. High-performance liquid chromatography was use to separate and collect gramicidins A, B, and C from gramicidin D (Sigma Chemical Co., St. Louis, MO) (*2*, *23*). Methanolic solutions of the separated gramicidins were chromatographed on Sephadex LH-20 (Pharmacia Fine Chemicals, Piscataway, NJ) to achieve further purity. The concentrations of the analogues purified in this manner were determined at 280 nm, on a Cary-210 UV spectrometer using extinction coefficients of 20 840, 15 260, and 18 600 M^{-1} (*24*) for gramicidins A, B, and C, respectively. Deuterated sodium dodecyl sulfate (d_{25}-SDS), deuterium oxide (D_2O), and deuterated trifluoroethanol (CF_3CD_2OH, d_2-TFE) were obtained from Cambridge Isotope Laboratories (Cambridge, MA). The d_{25}-SDS was recrystallized twice from 95% ethanol. A 100 mM phosphate buffer solution, pH 6.5, was purchased from PGC Scientifics (Gaithersburg. MD). NMR samples were prepared by combining 50 mM solutions of the gramicidin analogues dissolved in d_2-TFE with 275 mM aqueous d_{25}-SDS solution (89% pH 6.5 buffer/11% D_2O, v/v) to final concentrations of approximately 5 mM gramicidin analogue and 250 mM d_{25}-SDS in 80% pH 6.5 buffer/10% D_2O/10% d_2-TFE. These mixtures were sonicated for approximately 5 min to facilitate incorporation of gramicidin into the micelles. Circular dichroism spectra of each sample, obtained with a Jasco J-710 Spectropolarimeter (Jasco, Inc., Easton, MD) showed the characteristic maxima at 218 and 235 nm indicative of the $\beta^{6.3}$-helical dimer channel observed in dipalmityolphosphatidylcholine vesicles (*25*−*27*). A total of 400 μL of each sample was then transferred to 4 mm NMR tubes (Ultrahigh Precision, 535-PP, Wilmad, Buena, NJ). The one-dimensional ^1H NMR spectra of each sample, obtained with a Varian VXR 500S NMR (Varian, Inc., Palo Alto CA) spectrometer, showed no evidence of species heterogeneity (*28*, *29*).

Methods. (i) NMR Spectroscopy. All two-dimensional NMR experiments were performed using a Varian VXR 500S NMR spectrometer. The ^1H chemical shifts of each analogue were determined using the standard technique involving DQF-COSY, TOCSY, and NOESY experiments (*30*). A spectral width of 6000 Hz was used in both dimensions for each 2-D experiment. All spectra were recorded in the phase-sensitive mode (*31*) using the States, Ruben and Haberkorn method (*32*). Water suppression was achieved by transmitter presaturation. All experiments were performed at 55 °C.

The DQF-COSY spectra were acquired in 512 t_1 increments with 8192 or 16 384 t_2 data points to achieve high digital resolution. One hundred twenty-eight transients were used per t_1 increment.

The TOCSY spectra were acquired in 256 t_1 increments (64 transients/increment) with 4096 t_2 data points. The data for these experiments were acquired with a mixing time of 75 ms using the MLEV-17 mixing scheme (*33*).

The NOESY spectra were acquired in 512 t_1 increments (128 transients/increment) with 8192 t_2 data points. A delay of 2.7 s was used before the initiation of the pulse sequence. A mixing time of 40 ms was used to ensure that cross-peak volumes were within the linear region of NOE build-up.

(ii) Molecular Modeling Strategy. NOESY processing, peak volume measurements, and relaxation matrix calculations were accomplished using FELIX 95.0 (BIOSYM/MSI, San Diego, CA). The structure of each analogue was obtained using the distance geometry/simulated annealing (DG/SA) method (*34*) implemented in DSPACE 4.0 (Hare Research Inc., Woodinville, WA). The DSPACE software allows one to use molecular symmetry during the structure refinement of a dimer, an option necessary for modeling the complete gramicidin channel. Minimizations of the final structures were performed using DISCOVER 97.2, as supplied in the INSIGHT II 98.0, software package (BIOSYM/MSI, San Diego, CA). All calculations were run on 4D/25G and O2 Silicon Graphics computer systems (Silicon Graphics, Inc., Pittsford, NY).

Upper distance constraints were initially generated for each uniquely assignable peak in the NOESY spectra, using the methylene protons of Gly_2 as a reference. The lower distance constraints were set to the van der Waals contact distances for the atom pairs. All constraints involving methyl groups were corrected appropriately (*35*). The method of floating chiralities (*36*) was used to complete stereospecific assignments for all methylene protons. After several iterations of modeling both monomer and dimer structures, the distance constraints were further optimized with relaxation matrix calculations (*37*). This theoretical spectral analysis allowed verification of peak assignments and improvement of the set of distance constraints by resolving overlapped cross-peaks, and correctly quantifying the volumes for cross-peaks residing very close to the diagonal where t_1 ridge noise in the experimental spectrum often hides peaks or increases their size thus leading to erroneous distance constraints.

Gramicidin dimer channels are formed from a symmetrical, head-to-head association of monomeric helices (*13*, *14*); therefore, a great majority of the observed NOEs occur within a monomer. However, a number of the observed NOEs are

related to monomer−monomer interactions. Initial modeling was performed on a monomer structure to drastically lower computation time, since dimer matrixes are four times larger than monomer matrixes and thus the potential function would have required a 4-fold increase in computer time for evaluation. DSPACE was used to generate initial structures for each gramicidin analogue. New amino acid definition files for the D-amino acids were created by changing the chirality of the α carbons in the files of the corresponding L-amino acids. In addition, it was necessary to correct several improperly defined stereospecific assignments in the original definition files. During the initial modeling of GA, it was noted that half of the conformers generated had a final penalty function more than an order of magnitude greater than the others. It was determined that these structures resulted from mirror-image embeds generated by distance geometry. The solution to this problem was the insertion of a test for the handedness of the β-helix immediately after the embedding step in the DG/SA algorithm. This was accomplished using the signed volume equation normally used for determining chirality in distance geometry (*38*):

$$\text{signed volume} = 1/6(v_1 - v_4)[(v_2 - v_4) \times (v_3 - v_4)] \quad (1)$$

where v_1, v_2, v_3, and v_4 represent the position vectors of each of the atoms attached to the chiral center, and the sign of the volume indicates the chirality. A positive volume for the α carbons of residues Val_1, D-Leu_4, D-Leu_{12}, and D-Leu_{14} indicated a right-handed conformer. In cases where the volume had a negative sign, the coordinates were inverted prior to annealing, resulting in acceptable penalty values for all conformers at the completion of the DG/SA algorithm.

To obtain the final dimer structure, three hydrogen bond constraints and approximately 27 distance constraints for interactions between monomers were included. In addition, the C_2 symmetry of the dimer was defined and used in the refinement process, essentially doubling the number of constraints. DSPACE maintains symmetry by addition of a term to the force field. This term compares distances within the two monomers and introduces a penalty when they differ. Inclusion of these dimer interactions had a significant effect upon the previously determined monomer structure.

Dimer structures for GA, GB, and GC were modeled using a total of 13 hydrogen bonds and 547, 622, and 590 distance constraints, respectively. One hundred conformers were generated for the dimer of each analogue. Average structures were generated from the 10 best structures (i.e., 10 structures with the lowest penalty function), and these average structures were further optimized using DISCOVER. The constrained DISCOVER minimizations were performed using the all-atom AMBER force field and a dielectric constant of 2.0 (*39*, *40*) to emulate that of the micelle interior in which the peptide resides. One hundred iterations of steepest descent minimization were followed by conjugate gradient iterations until convergence criteria, maximum derivative of <0.001 kcal/Å, were met.

RESULTS

Although the cation binding and transport properties of GA, GB, and GC have been studied in detail, a comparison of the three-dimensional structure of these peptides has not been possible to date because structures were not available

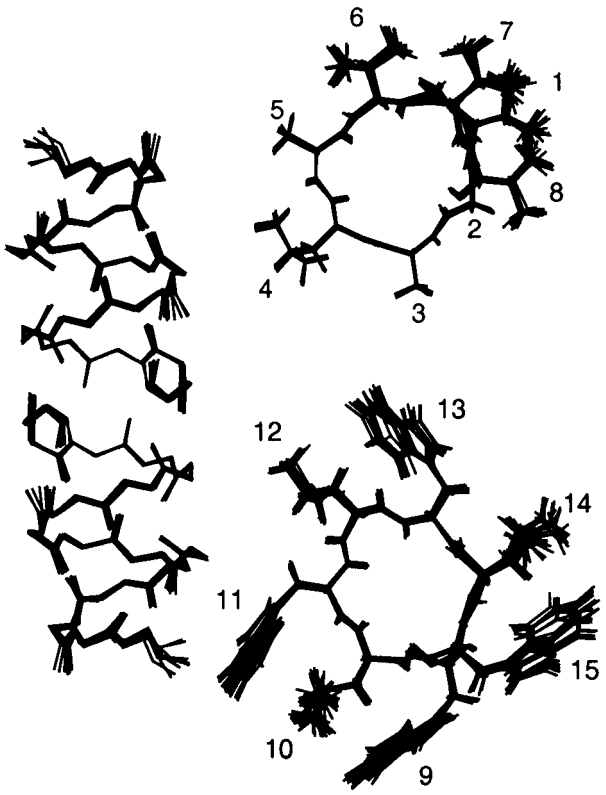

FIGURE 1: All-atom superposition of the 10 best dimers obtained for GA. (Left) Side view showing only the heavy atoms of the backbone for the entire dimer, including the formyl and ethanolamine capping groups. (Right) Two regions of a single monomer, residues Val_1 through D-Val_8 (top) and residues Trp_9 through Trp_{15} (bottom), shown from an end-on perspective to view side chains.

for GB and GC. Having been refined using distance constraints and a well-defined, widely used molecular force field, the final structures for GA, GB, and GC presented here represent the best possible conformations for the given experimental data. The quality of the structures generated for GA, GB, and GC can be shown in several ways. The visual superposition of the best set of structures for a given analogue is commonly used to judge their similarity. Figure 1 shows three views of the all-atom superposition of the 10 best dimer structures obtained for GA (similar results for GB and GC not shown). The backbone is shown for the entire dimer; however, to see side-chain orientations clearly, one monomer is separated into two components, residues Val_1 through D-Val_8 and residues Trp_9 through Trp_{15}. Root-mean-square deviations (RMSD) for atom positions have also been used to test the similarity of the 10 best and average structures for each analogue. Table 1 presents the average RMSD values for pairwise comparisons of each structure and comparisons of each structure to the average and minimized average structures (prior to the final DISCOVER minimization) for GA, GB, and GC. The ethanolamine group (Eta) has a high degree of conformational freedom, which results in fewer distance constraints restricting its position, as seen in Figure 1. To analyze the consistency of the amino acid positions, Eta has been omitted from the RMSD calculations. Typical RMSD values for published protein structures, determined using NMR spectroscopy and molecular modeling, are in the range of ~0.9 to ~1.75 Å for all heavy atoms and between ~0.30 and ~0.85 Å for compari-

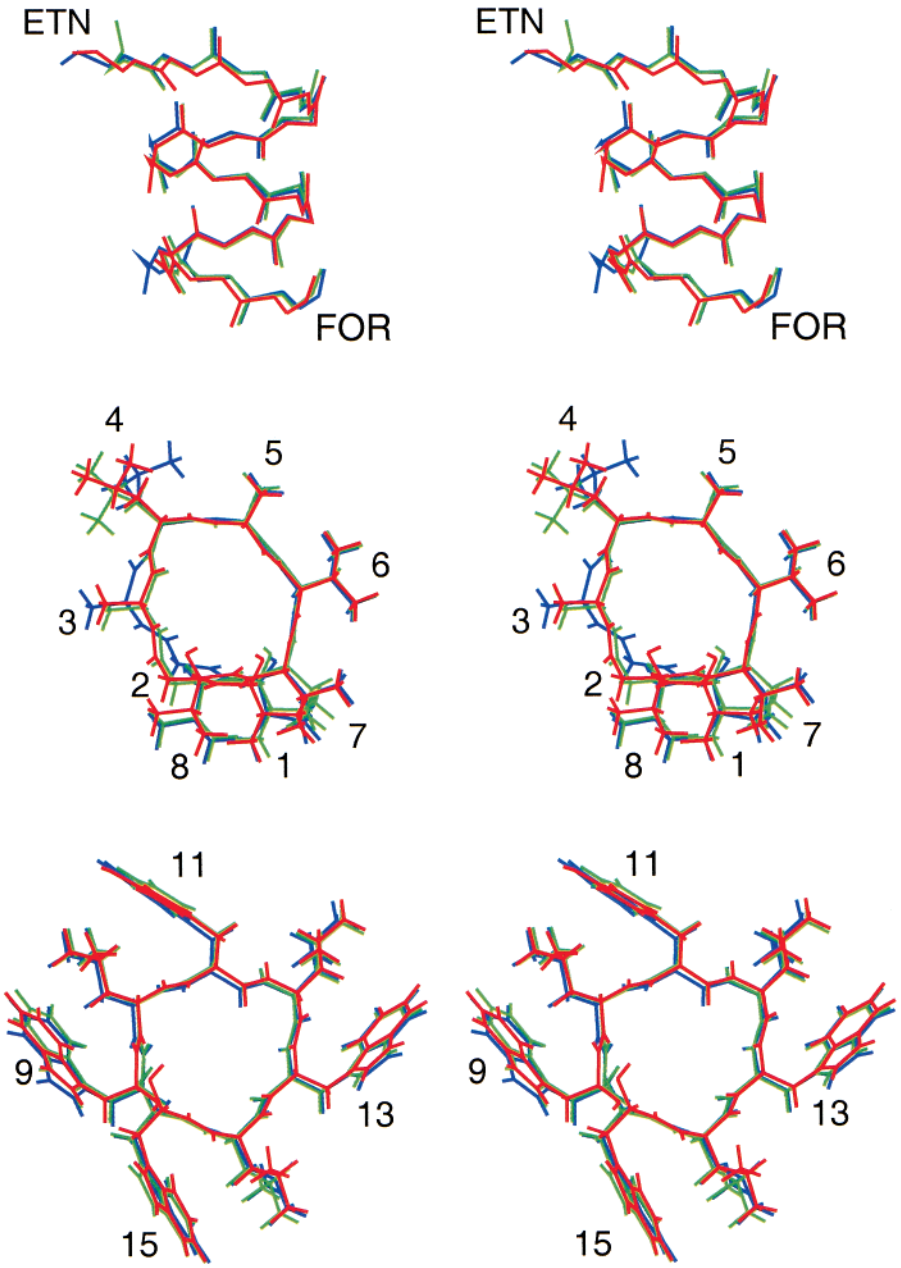

FIGURE 2: Divergent stereoviews showing the heavy-atom superposition of the final DISCOVER minimized structures of GA (blue), GB (green), and GC (red). The top image is a side view showing the heavy atoms of the backbone, including the formyl and ethanolamine capping groups, for one-half of the channel (monomer). The middle and bottom images are end-on views showing all atoms for residues Val_1 through D-Val_8 and residues Trp_9 through Trp_{15}, respectively. The formyl groups are aligned in all three figures.

son of backbone atoms (examples found in refs *41*−*47*). The structures of GA, GB, and GC are well characterized since the all-atom RMSD values are within or below the range of heavy-atom comparisons found in the literature and the heavy atom and backbone RMSD values fall within or below the published backbone statistics.

A comparison of the final DISCOVER minimized structures of GA, GB, and GC, using heavy-atom superposition, can be seen in Figure 2 where stereoviews of the backbone (one monomer only), residues Val_1 through D-Val_8, and residues Trp_9 through Trp_{15} are presented. The channels formed by the backbones of GA, GB, and GC are remarkably similar. The backbone atom RMSD values for GA/GB, GA/GC, and GB/GC are 0.45, 0.51, and 0.30 Å, respectively, and are within the accepted limits ascribed to similar structures.

Table 1: Average RMSD and Standard Deviations for the Ten Best and Average Structures of the Gramicidin Analogues Calculated Using Differences between Atomic Coordinates[a]

analog	comparison	all − Eta (Å)	heavy − Eta (Å)	backbone (Å)
GA	pairwise	0.71 ± 0.05	0.27 ± 0.05	0.21 ± 0.04
	vs avg	0.48 ± 0.02	0.18 ± 0.04	0.14 ± 0.03
	vs minimized avg	0.60 ± 0.04	0.19 ± 0.04	0.15 ± 0.04
GB	pairwise	1.02 ± 0.10	0.65 ± 0.13	0.43 ± 0.11
	vs avg	0.69 ± 0.06	0.44 ± 0.09	0.29 ± 0.06
	vs minimized avg	0.80 ± 0.06	0.46 ± 0.10	0.31 ± 0.10
GC	pairwise	1.10 ± 0.15	0.71 ± 0.14	0.51 ± 0.12
	vs avg	0.74 ± 0.11	0.48 ± 0.10	0.34 ± 0.08
	vs minimized avg	0.83 ± 0.14	0.49 ± 0.12	0.36 ± 0.08

[a] The minimized average structures used for these comparisons are not the final DISCOVER minimized structures.

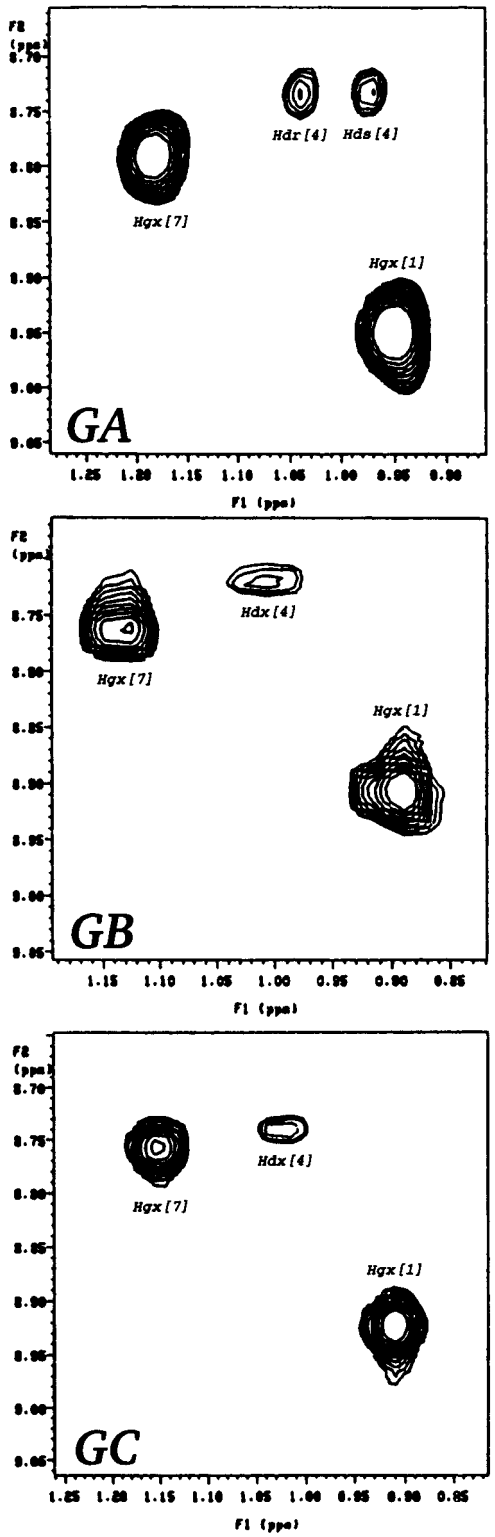

FIGURE 3: Region of the TOCSY spectra of GA, GB, and GC showing the lack of resolution of R and S methyl groups in Val_1, D-Leu_4, and Val_7. Key to peak labels $g = \gamma$; $d = \delta$; x is used when R and S are not resolved. For example, *Hdx[4]* labels the peak arising from the interaction of the H_N of D-Leu_4 with both H_δ methyl groups of D-Leu_4.

With a few exceptions, the conformations of the side chains for GA, GB, and GC are also consistent. The most notable exception involves D-Leu_4, and to a lesser extent, residues Val_7 and D-Leu_{14}. Apparent from the TOCSY spectra, portions of which are shown in Figure 3, the two δ methyl groups of D-Leu_4 are well resolved for GA but not for GB and GC. This suggests faster rotation about the χ_2 angle of this residue in GB and GC, creating magnetic equivalence for the two methyl groups. This could be explained by the presence of a larger side chain at position 11 in GA; the indole side chain of Trp_{11} in GA may restrict the rotation of the D-Leu_4 side chain. In fact, seven cross-peaks in the NOESY spectrum of GA were assigned as interactions between the side chains of Trp_{11} and D-Leu_4. Only one such interaction was assigned in the GB NOESY spectrum and no interactions of this type were observed for GC. Differences in the chemical shifts of $H_{\beta,R,S}$ and $H_{\delta,R,S}$ in D-Leu_4 observed for GA compared with GB and GC suggest minor conformational differences for this residue.

Significant motion in the side chains of Val_1 and Val_7 is indicated by the observation of only one chemical shift for the H_γ methyl groups of GA, GB, and GC (Figure 3). However, only the Val_7 residue of GB adopts a different conformation compared with GA and GC. The number and type of distance constraints obtained from the NOESY spectra determine conformational similarity and/or difference during molecular modeling. For Val_1, dimer constraints involving H_β have helped to secure a common configuration for all analogues. In contrast, the H_β of Val_7 in GB has only one constraint with Val_1 while both GA and GC have four and three, respectively, plus one constraint with Gly_2. This difference in distance constraints suggests a real, although quite small, variation in side-chain conformation for GB.

The chemical shifts of H_β, H_γ and H_δ of D-Leu_{14} do not indicate any conformational differences among the analogues; however, the orientation is different in GC. The cause can be traced back to the distance constraints used to define the position of this residue; four distance constraints between D-Val_8 and D-Leu_{14} and seven distance constraints between D-Leu_{14} and Trp_{15} are much different for GC than for GA or GB. It is difficult to ascertain why the change in amino acid at position 11 from Trp or Phe to Tyr would cause the observed conformational change in D-Leu_{14}.

The heavy-atom RMSD values, excluding Trp_{11}, Phe_{11}, Tyr_{11}, and Eta, are 0.69 Å for GA/GB, 0.69 Å for GA/GC, and 0.64 Å for GB/GC, quite small despite the minor configurational differences in the side chains of D-Leu_4, Val_7, and D-Leu_{14}. The RMSD values, for both backbone and heavy-atom comparisons, affirm a high degree of structural similarity for these three gramicidin analogues.

It should be noted that the positions of the indole rings of Trp_9, Trp_{13}, and Trp_{15} are the same in all three analogues. In addition, despite differences in size and polarity, the positions of the side chains of Trp_{11}, Phe_{11}, and Tyr_{11} are conserved, and the aromatic groups lie parallel in the superposition of GA, GB, and GC.

DISCUSSION

Comparison with Previously Published Structures of GA. In determining a molecular structure using an NMR technique, one must consider the nature and time scale of the motions within the molecule and how they relate to the time scale of the measuring technique (*48*). NMR spectroscopy has a relatively long time scale that can vary for different NMR techniques. If there is significant molecular motion over the time scale of the measurement, "the structure"

determined using the NMR data will be a motionally averaged structure. The term "structure" used here for GA, GB and GC actually represents the average of 10 averaged structures. Unless there are significant motional differences between GA, GB, and GC on a time scale faster than that of the NMR measurement, the comparison of these structures remains valid. However, a comparison of structures of GA determined by different NMR techniques would be expected to reveal some differences. Likewise, the structures of a molecule obtained by the same NMR technique but different molecular modeling protocols would not be identical.

The structure of the GA dimer channel has previously been reported by Arseniev et al. (*49*−*51*) and Cross et al. (*52*−*58*). The structure of GA published by Arseniev et al., like the structure presented here, was determined in SDS micelles using 2-D NMR spectroscopy and molecular modeling. While the GA:SDS ratio (1:50) and the temperature at which the NMR experiments were preformed (55 °C) were the same for both studies, there are a number of differences in data acquisition and molecular modeling protocol. For the NOESY experiment, Arseniev et al. used a 100 ms mixing time (*51*) which not only falls just outside of the linear portion of the NOE buildup curves determined experimentally in this lab, but more than doubles the time scale of the experiment compared with our use of 40 ms. Arseniev's et al. modeling protocol (*49*) constrained ϕ and χ dihedral angles using values derived from spin−spin coupling constants observed in the DQF-COSY spectrum and fixed all ω angles to 180°. Additionally, a hydrogen bond constraint was included between the carbonyl of D-Leu$_{10}$ and the hydroxyl group of Eta which tethered this capping group to the channel. Last, the structure was modeled only as a monomer; the dimer being assembled such that the hydrogen bonds and C_2 symmetry were satisfied.

In contrast to their procedure, we chose to model the gramicidin channel as a dimer using only hydrogen bond constraints and NOESY-derived distance constraints. The planarity of each peptide bond, governed by the ω dihedral angle, has been allowed to relax to a more natural, less strained conformation. We believe that the relatively few NOESY cross-peaks involving Eta indicate a high degree of conformational flexibility; therefore, the hydrogen bond constraint between D-Leu$_{10}$ and Eta has been omitted from our modeling calculations. Solid-state NMR studies of GA with deuterated Eta also indicate a high degree of conformational flexibility for this group (*59*). Modeling the gramicidin channel as a dimer, using experimentally determined dimer constraints, allowed the refinement of the monomer−monomer interface and the determination of its impact on the entire channel structure.

Despite the differences in the methods used, the structure of GA presented here and that of Arseniev et al. (the average of the five structures found in the RCSB PDB, code 1GRM) are quite similar, as can be seen in the various views of the superposition shown in Figure 4. Our use of a large number of dimer constraints during modeling creates obvious differences in the region between the monomers (i.e., Val$_1$ through D-Val$_6$). Interactions between Val$_1$ and D-Val$_6$ of opposite monomers pull the formyl group and the first residue away from the channel center and bring the backbone of Ala$_5$ and D-Val$_6$ toward the opposite monomer. The only side chain in this region that is affected by the dimer constraints is D-Leu$_4$. It is apparent from the stereoview of the overlay of the two structures that both χ_1 and χ_2 for this residue are quite different such that the δ hydrogens in our structure face the other monomer thus satisfying the dimer constraints. Without dimer constraints, the δ hydrogens of D-Leu$_4$ in the Arseniev et al. structure face the hydrogens in D-Leu$_{10}$. The RMSD values between the two average structures for the backbone and all heavy atoms are 0.73 and 3.13 Å, respectively. The backbone RMSD supports the similarity in channel structure while the heavy-atom RMSD reflects largely upon the conformational differences close to the dimer junction, especially of D-Leu$_4$, and of the Eta terminal group, both of which can be explained by differences in the molecular modeling strategies used by each group.

Cross et al. (*52*−*58*) have determined the structure of isotopically labeled GA incorporated into planar dimyristoylphosphatidylcholine (DMPC) bilayers using orientational constraints derived from solid-state NMR experiments. There are numerous experimental details that differ between the methods used by Cross et al. and those used in this study that could result in structural differences. For the solid-state NMR experiments, GA was incorporated into lipid bilayers made from zwitterionic DMPC molecules having a GA:DMPC ratio of 1:8. These bilayers were deposited onto glass slides from a benzene/ethanol solvent system, dried, and then rehydrated. To obtain orientational constraints, a number of solid-state NMR experiments were performed, with time scales varying over 2 orders of magnitude. All of the solid-state experiments were performed at or below 36 °C. The modeling protocol employed ^{15}N and ^{13}C anisotropic chemical shifts, ^{15}N-^{13}C dipolar splittings, quadrupolar splittings, N−O and H−O hydrogen bond distances, and the molecular energy as constraints.

In this study, spherical, negatively charged SDS micelles have been used as the membrane-mimetic environment. The aqueous solutions of these micelles has a GA:SDS ratio of 1:50 and also contains the 0.25M Na^+ associated with the detergent molecule. The time scale of the NOESY experiment is different from the multiple solid-state experiments performed with GA incorporated into bilayers. The variation in time scale, by orders of magnitude, of all of these experiments could result in subtle differences in structural parameters gathered from the individual experiments. Additionally, the solution state NMR experiments were performed at 55 °C, more than 20 °C higher than the solid-state experiments. Variations in molecular motions caused by this temperature difference could result in an average over different conformational space for each type of experiment. Again, the GA dimer was modeled using DG/SA and minimization constrained by C_2 symmetry, hydrogen bond distances and NOESY-derived distance constraints.

Figure 5 shows the overlay of the structure for GA presented here upon the solid-state structure (RCSB PDB, code 1MAG). The most significant conformational difference involves Trp$_9$; in the Cross et al. structure Trp$_9$ stacks with Trp$_{15}$, whereas Trp$_9$ is rotated toward D-Leu$_{10}$ in both our structure and that of Arseniev et al. because there are no cross-peaks in the NOESY spectrum of GA in aqueous micellar solution that support a stacked orientation of Trp$_9$ with Trp$_{15}$. The modeling method used for the solid-state constraints requires a choice of a most probable conformation for each side chain based on torsional energy (*54*). Similar

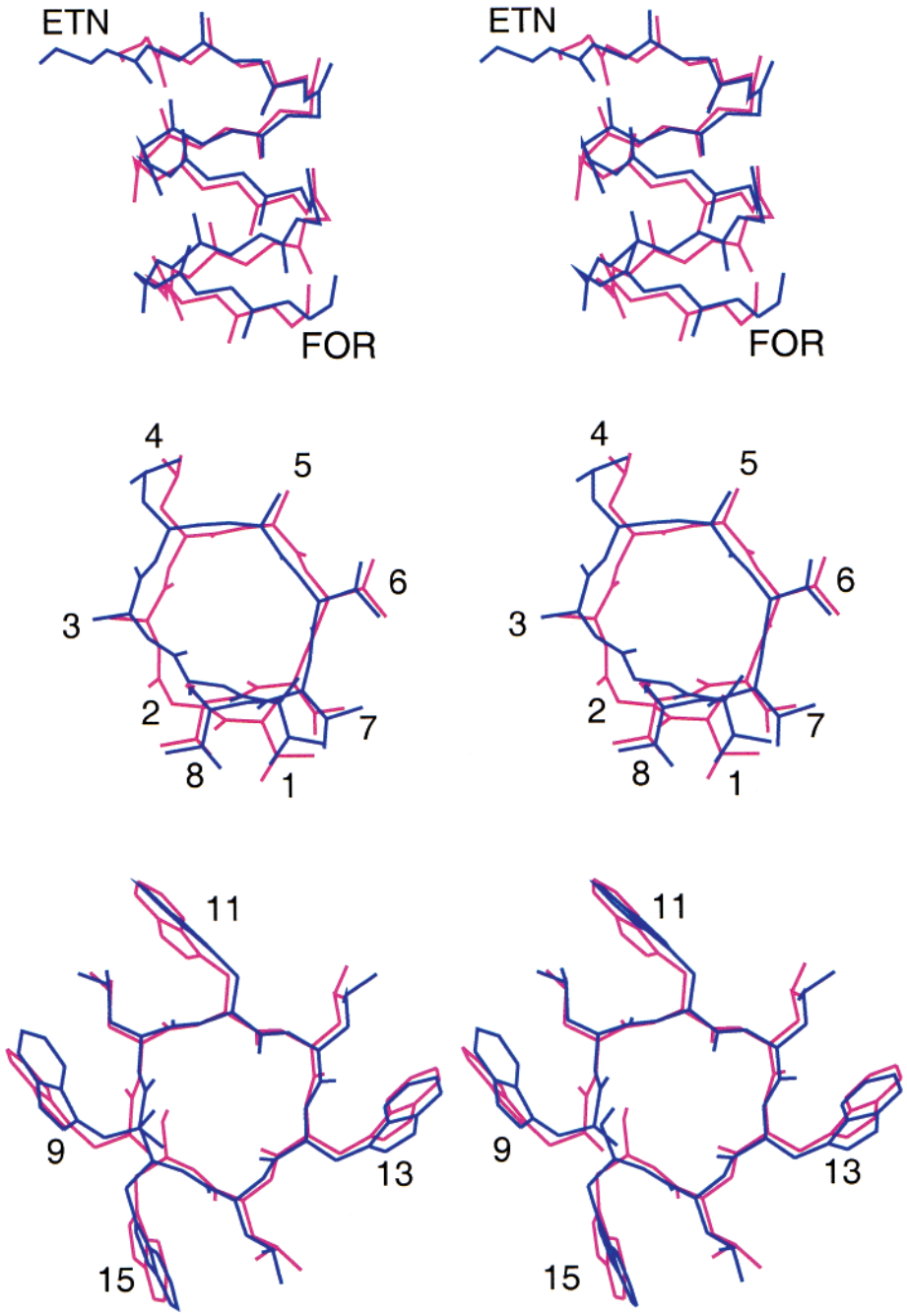

FIGURE 4: Divergent stereoviews showing the heavy-atom superposition of our final DISCOVER minimized structure of GA (blue) with the Arseniev et al. structure (purple; average of the five structures found in the RCSB PDB, code 1GRM). Coordinates for hydrogen atoms were not available for the Arseniev et al. structures; therefore, hydrogen atoms have been omitted from this figure. The top image is a side view showing the heavy atoms have been omitted from this figure. The top image is a side view showing the heavy atoms of the backbone, including the formyl and ethanolamine capping groups, for one-half of the channel (monomer). The middle and bottom images are end-on views showing heavy atoms for residues Val_1 through D-Val_8 and residues Trp_9 through Trp_{15}, respectively. The formyl groups are aligned in all three figures.

χ_1 and χ_2 dihedral angles were chosen for each of the four tryptophan residues so that each indole is oriented in the same direction to achieve maximum channel efficiency. This conformational choice was made because of the significant stacking energy created by the indoles. Cross has stated that, "...I agree that the NMR data that I presented are consistent with two Trp_9 conformational possibilities. We have no NMR data that support the structure in which Trp_{15} stacks with Trp_9. I would also like to point out there are a number of side chain structural differences, i.e. differences in rotameric state between the SDS structure and the lipid bilayer structure, so just because it exists in SDS in one conformation does not necessarily mean that it is present in the same conformation in bilayers" (*60*). However, several other groups (*61*−*63*) have presented solid-state NMR results for GA in lipid bilayers that are interpreted as being consistent with the nonstacking orientation presented here. Comparison of the Cross et al. structure with our structure shows that, in addition to Trp_9, only the D-Leu residues have largely different rotameric states. As with Trp_9, the conformations of the D-Leu residues in the solid state study were chosen as most probable based on torsional energy, whereas the

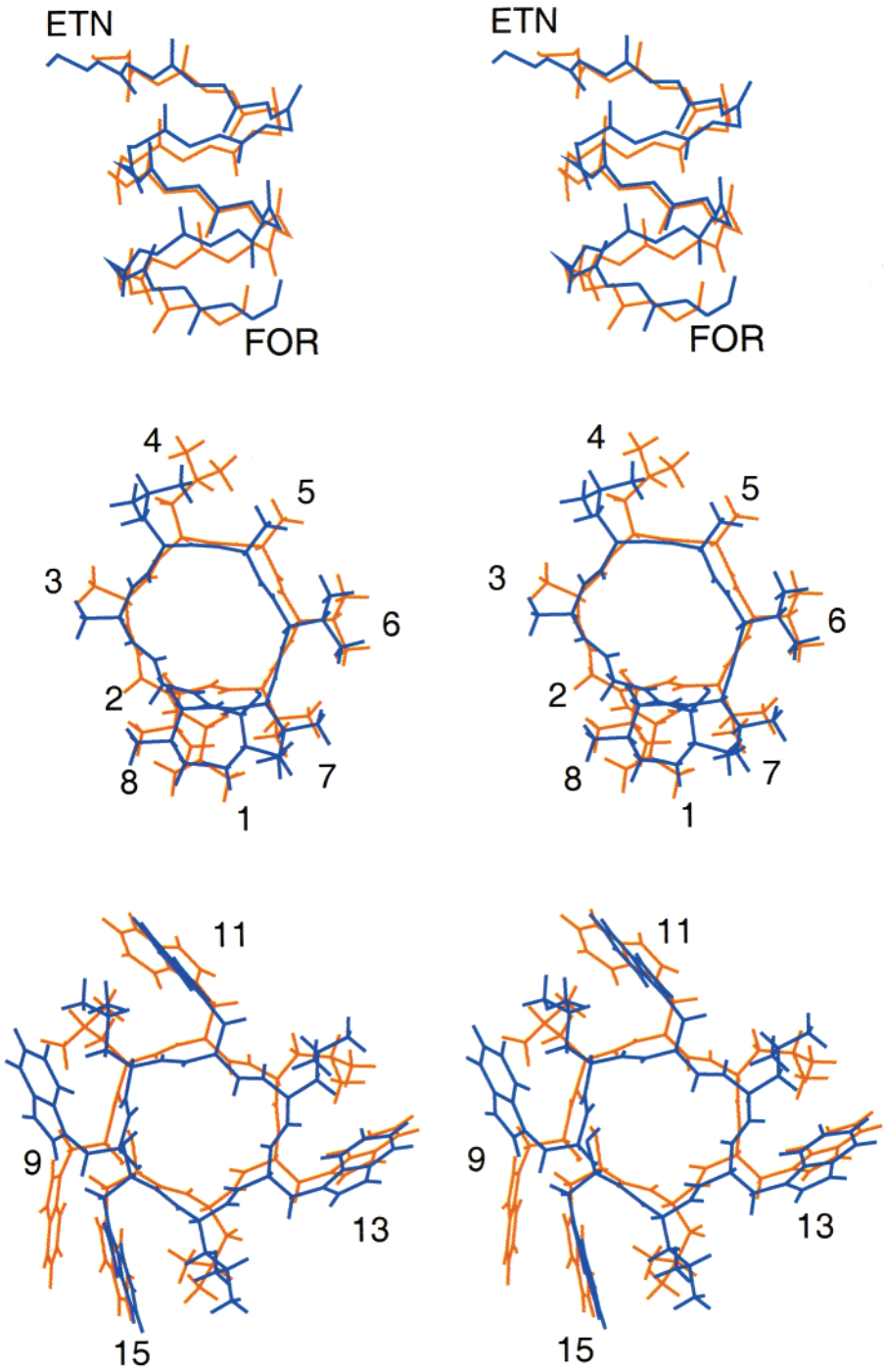

FIGURE 5: Divergent stereoviews showing the heavy-atom superposition of four final DISCOVER minimized structure of GA (blue) with the Cross et al. structure (orange; RCSB PDB, code 1MAG). The top image is a side view showing the heavy atoms of the backbone, including the formyl and ethanolamine capping groups, for one-half of the channel (monomer). The middle and bottom images are end-on views showing all atoms for residues Val_1 through D-Val_8 and residues Trp_9 through Trp_{15}, respectively. The formyl groups are aligned in all three figures.

structure presented here has been modeled using more than 60 NOESY derived distance constraints per D-Leu, including the dimer constraints that help to define the position of D-Leu_4.

Backbone and heavy-atom RMSD values for the comparison of the structures of GA in SDS with that in DMPC are 0.77 and 3.40 Å, respectively. The backbone RMSD value shows that channel structure is preserved in the two environments, while the differences in the conformations of the Trp_9 and the four D-Leu residues are responsible for the large heavy-atom RMSD. One must be cautious in interpreting this as structural dissimilarity because of the different physical states of the samples used in the solution and solid-state NMR experiments (e.g., curvature of SDS micelles vs planar DMPC bilayers, use of different peptide to detergent or lipid ratios, different headgroups, differences in the structure and dynamics of the hydrophobic/hydrophilic boundary in micelles and bilayers, different water contents), the different time frames in the NMR experiments, and the different protocols used for molecular modeling. The struc-

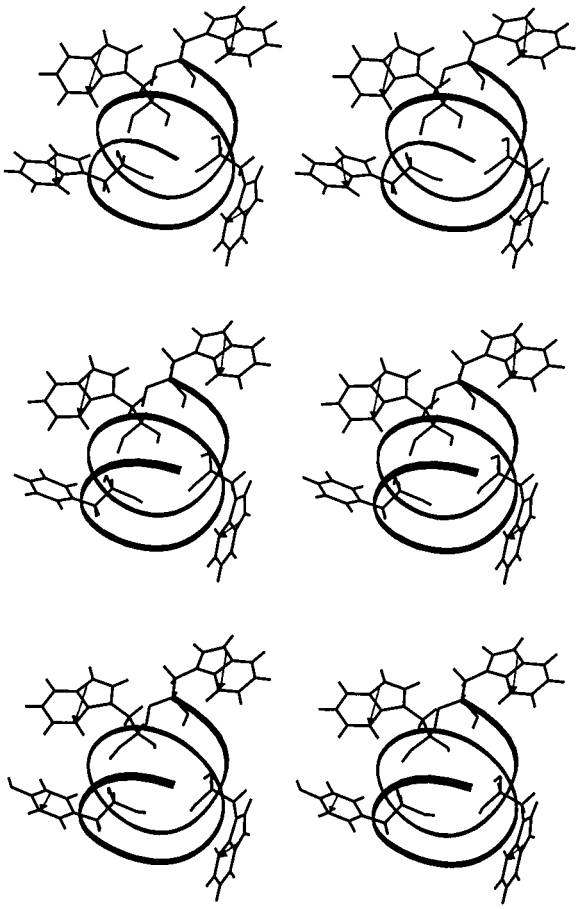

FIGURE 6: Divergent stereoviews showing the orientation of the dipole moments relative to the channel for the tryptophan and tyrosine side chains in GA (top), GB (middle) and GC (bottom). To simplify visualization, only monomers are shown and the channels are represented by ribbons. Following conventional representation, the arrowheads point in the direction of the negative poles.

ture presented here is thought to be a more accurate representation of the GA ion channel since it has been modeled as a dimer using a C_2 symmetry constraint, hydrogen bond constraints, and a set of distance constraints derived exclusively from experimental data.

Structure/Function Analysis of GA, GB, and GC. GA, GB, and GC differ by single amino acid substitutions located in the monovalent cation binding region of the channel. Replacement of Trp_{11} (dipole moment 2.08 D) in GA by Phe (dipole moment 0.0 D) in GB and Tyr (dipole moment 1.54 D) in GC affects binding enthalpies of monovalent cations to the channel, activation enthalpies of transport and single channel conductances. Without 3-D structures for each of these analogues, it has previously been impossible to determine if the differences in transport properties are caused by variations in side-chain orientations and/or backbone structure brought about by the mutations, or solely by changes in the magnitude and orientation of the dipole moment at the position of the mutation. With the structures for GA, GB, and GC presented here, an analysis of the structure/function relationship may now be possible.

The structural comparisons of GA, GB, and GC, discussed above, do not reveal conformational differences large enough to explain the variations in binding and transport observed for these gramicidin analogues. Figure 6 focuses on the orientation of the dipole moments of residues 9, 11, 13, and 15 relative to the channel for all three analogues. Together, Figures 2 and 6 show that the dipole moments for Trp_9, Trp_{13}, and Trp_{15} are aligned almost identically in each analogue with the negative poles pointing in the direction of the bilayer (or in this study micelle) interior in order to facilitate transport of the ion through the hydrophobic environment. Therefore, the differences in magnitude and orientation of the dipole moments of the amino acids substituted at position 11 must be responsible for altering ion-channel interactions. The negative pole of the Trp_{11} dipole in GA also points toward the bilayer interior; however, Phe_{11} in GB does not have a dipole moment, and the direction of the Tyr_{11} dipole moment in GC is not well-defined due to the probable rotational freedom of the hydroxyl group. In tyrosine, the direction of the dipole moment tracks the O−H bond in that the positive end of the dipole will follow the rotation of the hydrogen. The NMR experiments, unfortunately, do not provide the information necessary to determine a position for this group. The positions of both the O−H bond and the dipole moment shown in Figure 6 have been determined by molecular modeling and minimization. In this conformation, the dipole moment is situated with the negative end pointing toward the bilayer center but at an angle slightly different than for Trp_{11} in GA.

Table 2: Single Channel Conductances for Several Naturally Occurring and Synthetic Gramicidin Analogues[a]

analogue	Na^+ conductance (pS)
GA	14.4
GB	8.7
GC	13.3
Phe_9-GA	6.0
Phe_{11}-GA (GB)	8.7
Phe_{13}-GA	11.2
Phe_{15}-GA	10.9
5F-Trp_{11},Phe_9-GA	9.7
5F-Trp_9,Phe_{11}-GA	11.2

[a] NaCl (1.0 M) at 25 ± 1 °C and 200 mV in diphytanoylphosphatidylcholine/*n*-decane bilayers (*5*, *8*, *64*, *65*).

Additional evidence that ion−dipole interactions govern cation transport in gramicidin analogues is provided by analysis of single channel conductance measurements for singly and doubly substituted synthetic analogues (Table 2). Detailed information about channel backbone or side-chain conformations is not available for these synthetic analogues; however, hybrid channel formation with GA shows that these analogues adopt the $\beta^{6.3}$-helical structure (*8*, *64*, *65*), and conservation of the bulk and aromaticity of the substituted side chain(s) suggests a negligible impact on conformation (based on the comparisons of GA, GB, and GC). The loss of the tryptophan dipole in all of the analogues containing single Phe substitutions considerably decreases the single channel conductances. The conductance data also show a dependence on the position of the Phe substitution; i.e., the farther into the bilayer interior the dipole moment is located, the greater the impact when it is removed (Phe_9 > Phe_{11} > Phe_{13},Phe_{15}). As expected, multiple Trp to Phe substitutions compound the effect and further decrease cation transport (*8*, *64*). Single channel conductances have also been increased using enhanced side chains (*65*). Fluorination of the tryptophan indole at the C_5 position has a minor effect on the direction of the dipole moment, but increases the

magnitude from 2.08 to 3.64 D (*66*). The conductances of 5F-Trp$_{11}$,Phe$_9$-GA and 5F-Trp$_9$,Phe$_{11}$-GA increase by 30−60% compared with their parent molecules, Phe$_9$-GA and Phe$_{11}$-GA.

Thus, from the conductance, cation binding, and transport data, we find that there is a complex interplay between the dipole moments of the side chains and the ions being transported through the channel. The lack of conformational differences for GA, GB, and GC suggests that the magnitude and orientation of the side-chain dipoles is responsible for variations observed in the transport properties of gramicidin analogues.

SUPPORTING INFORMATION AVAILABLE

Chemical shifts for all ^{1}H in GA, GB, and GC. This material is available free of charge via the Internet at http://pubs.acs.org.

REFERENCES

1. Sarges, R., and Witkop, B. (1965) *J. Am. Chem. Soc. 87*, 2011.
2. Koeppe, R. E., II, Paczkowski, J. A., and Whaley, W. L. (1985) *Biochemistry 24*, 2822.
3. Koeppe, R. E., II, Corder, R. A., Andersen, O. S., Narcessian, E. J., Peart, L. M., and Waller, G. R. (1988) *Biophys. J. 53*, 328a.
4. Williams, L. P., Narcessian, E. J., Andersen, O. S., and Koeppe, R. E., II, (1988) *Biophys. J. 53*, 329a.
5. Williams, L. P., Narcessian, E. J., Andersen, O. S., Waller, G. R., Taylor, J., Lazenby, J. R., Hinton, J. F., and Koeppe, R. E., II (1992) *Biochemistry 31*, 7311.
6. Hotchkiss, R. D., and Dubos, R. J. (1941) *J. Biol. Chem. 141*, 155.
7. Ramachandran, L. K. (1975) *Biochem. Rev. 46*, 1.
8. Mazet, J.-L., Andersen, O. S., and Koeppe, R. E., II (1984) *Biophys. J. 45*, 263.
9. Russell, E. W. B., Weiss, L. B., Navetta, F. I., Koeppe, R. E., II, and Andersen, O. S. (1986) *Biophys. J. 49*, 673.
10. Weiss, L. B., and Koeppe, R. E., II, (1985) *Intl. J. Pept. Res. 26*, 305.
11. Hinton, J. F. (1999) in *Annual Reports on NMR Spectroscopy* (Webb, G. A., Ed.) Vol. 38, pp 89−120, Academic Press, London.
12. Hladky, S. B., and Haydon, D. A. (1970) *Nature 225*, 451.
13. Urry, D. W. (1971) *Proc. Natl. Acad. Sci. U.S.A. 68*, 672.
14. Arseniev, A. S., Barsukov, I. L., Bystrov, V. F., Lomize, A. L., and Ovchinnikov, Y. A. (1985) *FEBS Lett. 186*, 168.
15. Meyers, V. B., and Haydon, D. A. (1972) *Biochim. Biophys. Acta 274*, 313.
16. Sawyer, D. B., Williams, L. P., Whaley, W. L., Koeppe, R. E., II, and Andersen, O. S. (1990) *Biophys. J. 58*, 1207.
17. Bamberg, E., Noda, K., Gross, E., and Lauger, P. (1976) *Biochim. Biophys. Acta 449*, 223.
18. Hinton, J. F., Newkirk, D. K., Fletcher, T. G., and Shungu, D. C. (1994) *J. Magn. Reson. B 105*, 11.
19. Hinton, J. F., Fernandez, J. Q., Shungu, D. C., Whaley, W. L., Koeppe, R. E., II, and Millett, F. S. (1988) *Biophys. J. 54*, 527.
20. Hinton, J. F., and Koeppe, R. E., II, (1985) in *Metal Ions in Biological Systems* (Sigel, H., Ed.) Vol. 19, pp 173−200, Marcel Dekker, New York.
21. Hinton, J. F. (1996) *J. Magn. Reson. Ser. B 112*, 26.
22. Jude, A. R., Greathouse, D. V., Koeppe, R. E., II, Providence, L. L., and Andersen, O. S. (1999) *Biochemistry 38*, 1030.
23. Koeppe, R. E., II, and Weiss, L. B. (1981) *J. Chromatogr. 208*, 414.
24. Turner, G. L., Hinton, J. F., Koeppe, R. E., II, Parli, J. A., and Millett, F. S. (1983) *Biochim. Biophys. Acta 756*, 133.
25. Urry, D. W., Trapane, T. L., and Prasad, K. U. (1983) *Science 221*, 1064.
26. Spisni, A., Pasquali-Ronchetti, I., Casali, L., Linder, L., Cavatorta, P., Masotti, L., and Urry, D. W. (1983) *FEBS. Lett. 102*, 321.
27. Prasad, K. U., Trapane, T. L., Busath, D., Szabo, G., and Urry, D. W. (1983) *Int. J. Pept. Protein Res. 22*, 341.
28. Hinton, J. F., and Washburn, A. M. (1995) *Biophys. J. 69*, 435.
29. Hinton, J. F., Washburn, A. M., Snow, A., and Douglas, J. (1997) *J. Magn. Reson. 124*, 132.
30. Wüthrich, K. (1986) *NMR of Proteins and Nucleic Acids*, John Wiley and Sons, New York.
31. Bodenhausen, G., Kogler, H., and Ernst, R. R. (1984) *J. Magn. Reson. 58*, 370.
32. States, D. J., Haberkorn, R. A., and Ruben, D. J. (1982) *J. Magn. Reson. 48*, 286.
33. Bax, A., and Davis, D. G. (1985) *J. Magn. Reson. 65*, 355.
34. Nilges, M., and Clore, G. M., and Gronenborn, A. M. (1988) *FEBS Lett. 229*, 317.
35. Wüthrich, K., Billeter, M., and Braun, W. (1983) *J. Mol. Biol. 169*, 949.
36. Weber, P. L., Morrison, R., and Hare, D. (1988) *J. Mol. Biol. 204*, 483.
37. Keepers, J. W., and James, T. L. (1984) *J. Magn. Reson. 57*, 404.
38. Crippen, G. M. (1981) *Distance Geometry and Conformational Calculations*, Research Studies Press.
39. Brockman, H. (1994) *Chem. Phys. Lipids 73*, 57.
40. Plant, A. L., Gueguetchkeri, M., and Yap, W. (1994) *Biophys. J. 67*, 1126.
41. Zhou, H., Mazzulla, M. J., Kaufman, J. D., Stahl, S. J., Wingfield, P. T., Rubin, J. S., Bottaro, D. P., and Byrd, R. A. (1998) *Structure 6*, 109.
42. Goodfellow, B. J., Rusnak, F., Moura, I., Domke, T., and Moura, J. J. G. (1998) *Protein Sci. 7*, 928.
43. Drohat, A. C., Tjandra, N., Baldisseri, D. M., and Weber, D. J. (1999) *Protein Sci. 8*, 800.
44. Polshakov, V. I., Birdsall, B., Frenkiel, T. A., Gargaro, A. R., and Feeney, J. (1991) *Protein Sci. 8*, 467.
45. Monaco, V., Locardi, E., Formaggio, F., Crisma, M., Mammi, S., Peggion, E., Toniolo, C., Rebuffat, S., and Bodo, B. (1998) *J. Pept. Res. 52*, 261.
46. Yan, C., Digate, R. J., and Guiles, R. D. (1999) *Biopolymers 49*, 55.
47. Peng, Z.-H. (1999) *Biopolymers 49*, 565.
48. Davis, J. H., and Auger, M. (1999) *Progr. NMR Spectrosc. 35*, 1.
49. Arseniev, A. S., Lomize, A. L., Barsukov, I. L., and Bystrov, V. F. (1990) *Biol. Mem. 3*, 1723.
50. Lomize, A. L., Orekhov, V. Y., and Arseniev, A. S. (1992) *Bioorg. Khim. 18*, 182.
51. Arseniev, A. S., Barsukov, I. L., Bystrov, V. F., and Ovchinnikov, T. A. (1990) *Biol. Mem. 3*, 593.
52. Ketchem, R. R., Lee, K.-C., Huo, S., and Cross, T. A. (1996) *J. Biomol. NMR 8*, 1.
53. Ketchem, R. R., Roux, B., and Cross, T. A. (1997) *Structure 5*, 1655.
54. Cross, T. A. (1997) *Methods Enzymol. 289*, 672.
55. Tian, F., Lee, K.-C., Hu, W., and Cross, T. A. (1996) *Biochemistry 35*, 11959.
56. Ketchem, R. R., Hu, W., and Cross, T. A. (1993) *Science 261*, 1457.
57. Mai, W., Hu, W., Wang, C., and Cross, T. A. (1993) *Protein Sci. 2*, 532.
58. Kovacs, F., Quine, J., and Cross, T. A. (1999) *Proc. Natl. Acad. Sci. U.S.A. 96*, 7910.
59. Koeppe, R. E., Vogt, T. C., Greathouse, D. V., Killian, J. A., and de Kruijff, B. (1996) *Biochemistry 35*, 3641.
60. Cross, T. A. (1999) in *Gramicidin and Related Ion Channel-Forming Peptides* (Wallace, B. A., Ed.) Norvartis Foundation Symposium 225, p 18, John Wiley & Sons, New York.
61. Koeppe, R. E., II, Killian, J. A., and Greathouse, D. V. (1994) *Biophys. J. 66*, 14.
62. Separovic, F., Hayamizu, K., Smith, K., and Cornell, B. A. (1991) *Chem. Phys. Lett. 181*, 157.

63. Cornell, B. A., Separovic, F., Baldassi, A. J., and Smith, R. (1988) *Biophys. J. 53*, 67.
64. Becker, M. D., Greathouse, D. V., Koeppe, R. E., II, and Andersen, O. S. (1991) *Biochemistry 30*, 8830.
65. Anderson, O. S., Greathouse, D. V., Providence, L. L., Becker, M. D., and Koeppe, R. E., II, (1998) *J. Am. Chem. Soc. 120*, 5142.
66. Busath, D. D., Thulin, C. D., Hendershot, R. W., Phillips, L. R., Maughan, P., Cole, C. D., Bingham, N. C., Morrison, S., Baird, L. C., Hendershot, R. J., Cotton, M., and Cross, T. A. (1998) *Biophys. J. 75*, 2830.

BI010942W